Contribution of extra-hepatic aldehyde oxidase activity to human clearance

Kirk D. Kozminski, Jangir Selimkhanov, Scott Heyward, and Michael A. Zientek

Takeda Pharmaceuticals Limited, San Diego, CA (KDK, JS, MAZ)

BioIVT, Baltimore, MD (SH)

Drug Metabolism and Disposition

Manuscript number DMD-AR-2020-000313R1

In order to accurately estimate intrinsic clearance using available 4-oxo-carbazeran data, we wanted to precisely capture enzyme activity in each tissue's S9 fraction immediately upon initiation of the reaction with carbazeran. We observed that the rate of 4-oxo-carbazeran formation slowed significantly in all S9 incubations, which Abassi et al., 2019, attributed to inactivation of the AOX enzyme. Thus, to fit the non-linear rate of 4-oxo-carbazeran, we leveraged the AOX modulated activity model (MAM) developed by Abassi et al., 2019. The model (Figure 2) describes product (P) formation from substrate (S) by enzyme (E) through the formation of the enzyme-substrate complex (ES), which also leads to the formation (k_{inact}) of a less catalytically active version of the enzyme E* ($k_{cat,slow}<k_{cat,fast}$). The substrate and enzyme binding (k_{on}) and dissociation (k_{off}) rate constants are unaffected by the change in the enzyme's catalytic activity.

To fit MAM to 4-oxo-carbazeran data across multiple tissues, we initially assumed that all model kinetic parameters were the same across all tissues. This assumption implies that the AOX enzyme activity is unaffected by the potential differences across different tissue milieu. This assumption allows for the estimation of initial active enzyme activity in the intestinal S9 fraction, where product formation was observed only at high substrate concentrations (Figure 3). Additionally, the specific assumption that $k_{cat,fast}$ is the same across all tissue allows us to estimate active enzyme abundances across different tissues. Under this assumption, however, the model was not able to capture liver and kidney 4-oxo-carbazeran time course data sufficiently well (Figure S1).

To achieve a better fit to the data, we decided to relax the assumption that all model kinetic parameters had to be the same across all tissues. In order to determine which parameters had to be tissue-specific, we fit each of the well characterized tissues (all excluding intestine due to limited 4-OH formation) independently (Table S1 and Figure S2). We found that K_M, k_{inact}, and $k_{cat,slow}$ for higher substrate-turnover tissues, liver and kidney, were significantly different from those with lower substrate turnover, lung and vasculature. Furthermore, K_M appeared to be similar between kidney and liver. Therefore, we decided to introduce a shared k_{off} ($K_{M,tissue} = \frac{k_{on}+k_{cat,fast}}{k_{off,tissue}}$) parameter specific to liver and kidney as well as liver-specific and kidney-specific k_{inact} and $k_{cat,slow}$ parameters (Table 2). These changes resulted in a much improved model fit to the data (Figure 3), which did not appear significantly different from individual model fits (Figure S2). Based on the Akaike information criterion (AIC), the updated model (AIC = 491) significantly outperformed the initial model (AIC = 609).

Table S1: Modulated Activity Model individual tissue parameter estimates

Parameter	Liver	Kidney	Lung	Vasculature	Units
k_{on}	1.1E+07	1.7E+08	6.0E+07	7.9E+07	μM-1min-1
k_{off}	7.3E+07	8.1E+08	1.1E+09	1.5E+09	min-1
$k_{cat,fast}$	252	72	230	119	min-1
k_{inact}	0.42	0.15	1.1	0.88	min-1
$k_{cat,slow}$	6.2	11	9.8	5.1	min-1
E_{tissue}	1.7	0.082	0.031	0.089	pmol/mg S9
K_m	6.8	4.7	19	19	μM
V_{max}	420	5.9	7.1	11	pmol/min/mg S9

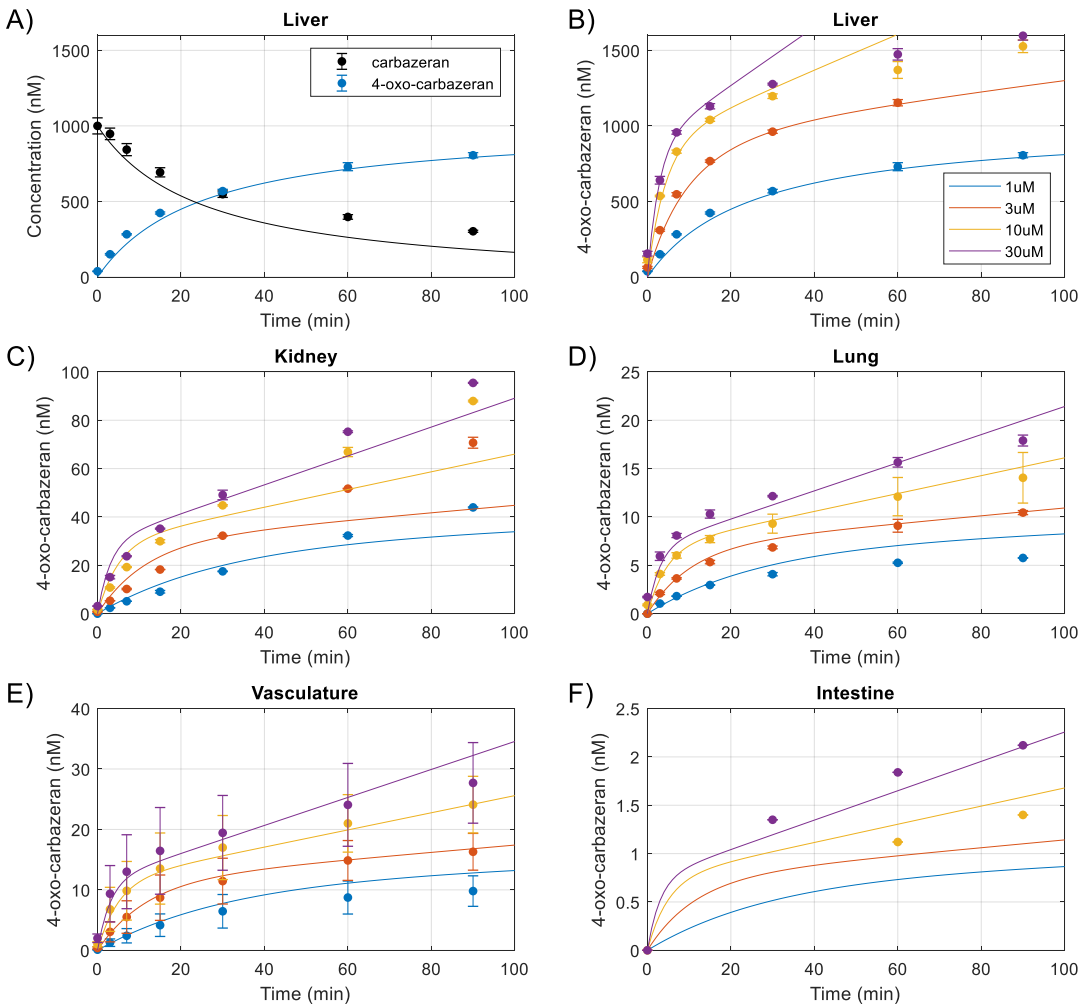

Figure S1. Time course of carbazeran depletion and 4-oxo-carbazeran formation in liver S9 fraction after incubation with 1 µM carbazeran (A). Time course of 4-oxo-carbazeran formation after incubation with 1 µM (blue), 3 µM (red), 10 µM (yellow), 30 µM (purple) carbazeran in liver (B), kidney (C), lung (D), vasculature (E), and intestinal (F) S9 fractions. Points represent average data with error bars representing standard errors associated with technical and biological (vasculature only) replicates. The curves show AOX modulated activity model simulations based on simultaneous fit to 4-oxo-carbazeran time course data from all tissue S9 fractions.

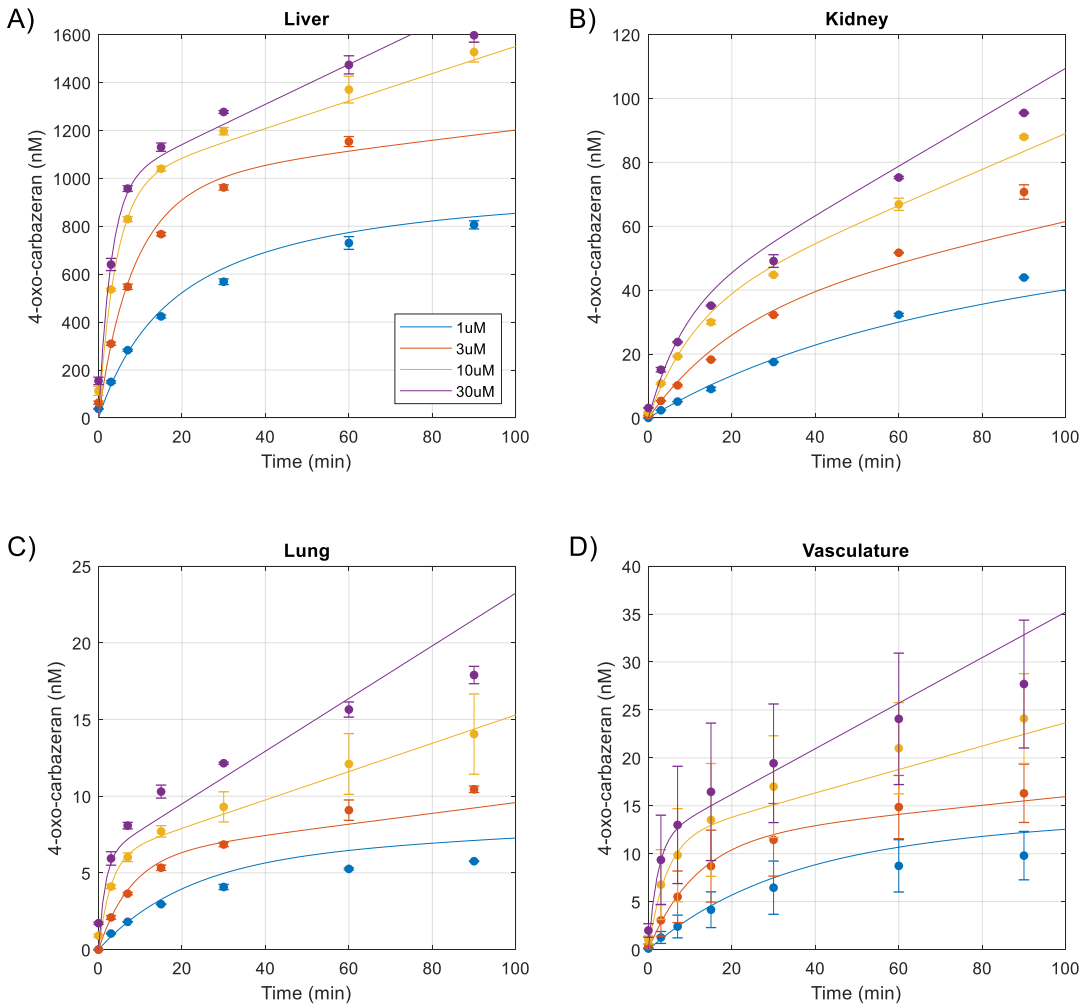

Figure S2. Time course of 4-oxo-carbazeran formation after incubation with 1 µM (blue), 3 µM (red), 10 µM (yellow), 30 µM (purple) carbazeran in liver (A), kidney (B), lung (C), and iliac arterial vasculature (D) S9 fractions. Points represent average data with error bars representing standard errors associated with technical and biological (vasculature only) replicates. The curves show AOX modulated activity model simulations based on simultaneous fit to individual tissue's S9 fraction 4-oxo-carbazeran time course data.

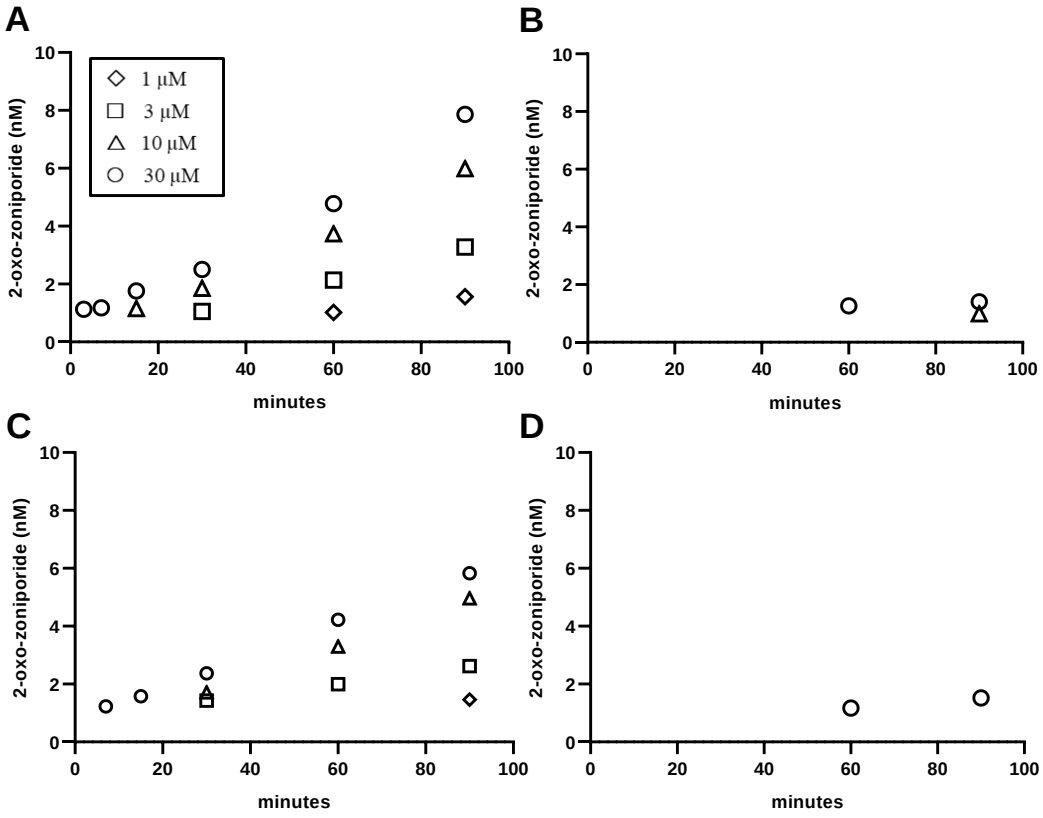

Figure S3. Time course of 2-oxo-zoniporide formation in kidney (A), lung (B), vasculature (C), and intestinal (D) S9 fractions (1 mg/mL) after incubation with 1 µM (◇), 3 µM (□), 10 µM (△), and 30 µM (○) zoniporide.